Proceedings of the XXXVI Zakopane School of Physics, Zakopane 2001

Materials Surface Processing Spied by Hyperfine Interactions

P. Schaaf[a,*], M. Weisheit[b] and H.-U. Krebs[b]

[a]Universität Göttingen, Zweites Physikalisches Institut und SFB 345
Bunsenstrasse 7/9, 37073 Göttingen, Germany
[b]Universität Göttingen, Institut für Materialphysik und SFB 345
Hospitalstrasse 5, 37073 Göttingen, Germany

There are many aspects of materials surface processing ranging from simple heat treatments to ion implantation or laser surface treatments, e.g. the laser-plasma-coating formation in nitrogen gas, which is called laser nitriding. These methods are often very complicated, involving many basic processes and they have to be optimised for the desired application. Nuclear methods can be successfully applied for this task. First, Ag/Fe multilayers can be prepared by pulsed laser deposition employing an excimer laser. The Ag/Fe system is immiscible and sharp interfaces are expected for that reason. Nevertheless, it will be presented that some intermixing occurs which can be seen by conversion electron Mössbauer spectroscopy with the additional trick of preparing a sensitive ^{57}Fe layer at various distances from the interfaces. Several Ag neighbours to the Fe spy-atom can be resolved, whose abundances vary with the location of the ^{57}Fe marker layer. It is found that the intermixing at the bottom and top interface of the Fe layers is asymmetric.

PACS numbers: 61.18.Fs

1. Introduction

Lasers have been more and more established in materials processing [1–3]. Recently, laser nitriding has been intensively studied [4, 5]. There, irradiating materials with short laser pulses in a reactive gas at high pressure may induce coating formation. With that, surface nitride layers of the irradiated material can be produced (Fe_2N, TiN, AlN) [2, 6–8]. The processes and resulting coatings have been

*corresponding author; e-mail: pschaaf@uni-goettingen.de

investigated employing a combination of nuclear methods (Rutherford backscattering spectrometry (RBS), resonant nuclear reaction analysis (RNRA)) making intensive use of hyperfine interactions (Mössbauer spectroscopy) [9–13].

Another laser application is pulsed laser deposition (PLD), which has developed to a powerful method for the preparation of well-defined surface layers [14–17]. Here, we present the PLD of Ag/Fe multilayers and the investigation of the resulting interfaces by Mössbauer spectroscopy (MS), X-ray diffraction (XRD) and Auger electron spectroscopy (AES). It is found that the interface intermixing is asymmetric with regard to the top and bottom interfaces.

2. Experimental

The multilayers have been prepared by PLD employing a UHV chamber and a KrF excimer laser (248 nm, $t_p = 30$ ns). The multiple-target/multiple-substrate set-up is described in Refs. [15–17]. High purity Ag and Fe targets have been used for the Ag/Fe multilayer production. Additionally, also a highly enriched ^{57}Fe foil has been used (isotope enrichment $> 95\%$) as target material. Thus, thin (0.5 nm) ^{57}Fe marker layers could be embedded into each of the natural iron layers in a well-defined distance from all the interfaces. The energy density on the target was set in such a way that the growth rate at the Si(111) substrate at a distance of 60 cm was 2.5 pm/pulse for Ag and 5 pm/pulse for Fe. It should be noted that the ions and atoms reach the substrate with energies in the range of 10 to 200 eV [15, 17]. The chamber also contains an AES spectrometer, so that the produced surface films can be analysed *in situ* by AES. XRD (large angle scattering) was used *ex situ* to quantify the interface quality by the satellite peaks resulting from the superstructure of the multilayers [15–17].

Accurate analysis of the short-range order of the ^{57}Fe spy-atoms was enabled by conversion electron Mössbauer spectroscopy (CEMS). The ^{57}Fe enrichment facilitated the measurement of the conversion electrons. The escape range of about 150 nm [18] is well suited for the total thickness of the multilayers being 100 nm. A constant acceleration drive and a ^{57}Co/Rh source of about 400 MBq activity were employed, together with a He/CH_4 gas-flow CEMS detector, integrally detecting all conversion and Auger electrons escaping from the sample surface [19]. The data were stored in a 1024 channels multiscaler and analysed by the WINISO program [20] by superimposing Lorentzian lines. Calibration was done with an α-Fe foil of 25 μm thickness, and isomer shifts are related to this calibration material.

3. Results and discussion

The general feature of the multilayers is represented in the CEMS spectra shown in Fig. 1. There, two multilayer samples are shown with periodicities of $\lambda = 3.8$ nm (20 periods) and $\lambda = 2.3$ nm (40 periods). Here, the periodicity

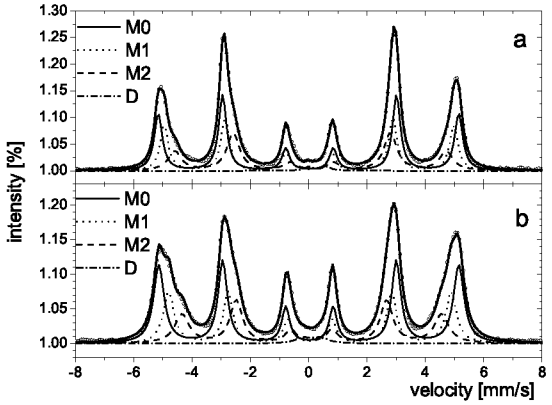

Fig. 1. CEM spectra of Ag/Fe multilayers: (a) 20 periods of $\lambda = 3.8$ nm, (b) 40 periods of $\lambda = 2.3$ nm. (only enriched ^{57}Fe used).

represents the sum of the Fe and Ag single-layer thickness (equal thickness of Ag and Fe) $\lambda = d_{\mathrm{Ag}} + d_{\mathrm{Fe}}$.

The spectra are fitted with three sextets (M0, M1, M2) and one doublet (D). The doublet D (with parameters $\delta = 0.20(5)$ mm/s, $\varepsilon = 0.60(3)$ mm/s) represents Fe-atoms in an Ag rich surrounding (Ag $> 30\%$), in accordance to the previous measurements [16, 21–24]. The magnetic subspectra M0 to M1 correspond to the bcc-Fe phase, where some Ag atoms are substitutionally incorporated, giving rise to some Fe-atoms having one, two or even more Ag atoms in the direct neighbourhood. The hyperfine fields are linearly decreasing with the number of nearest neighbour Ag-atoms [16, 21–24]. The mean values are 32.0(1) T (M0), 30.5(3) T (M1), and 28.3(5) T (M2). Thus, M0 corresponds to Fe atoms having no direct Ag neighbour, M1 having one and M2 having two or more Ag neighbours. The hyperfine fields are also influenced by the layer thickness and the overall Ag concentration in the bcc-Fe phase (influence of more distant Ag neighbours). The relative abundance of the sextets M1 and M2 is slightly increasing for the multilayer with the smaller periodicity. This means that there is more Ag in the bcc-phase, i.e. there is more intermixing. This is in accordance with the results of the X-ray measurements. Moreover the intensity ratios are changing with the periodicity. For $\lambda = 3.8$ nm all subspectra have their orientation in the layer plane. For $\lambda = 2.3$ nm the orientation of the M0 and M1 subspectra are re-orienting more towards a random orientation.

Figure 2 shows the CEM spectra for a Fe/Ag multilayer with a periodicity of $\lambda = 5$ nm. There, a ^{57}Fe marker layer of 0.5 nm thickness was introduced into each natural Fe layer, where its location was changed in 0.5 nm steps from the bottom interface to the top interface. Thus, the information collected by the CEM spectra originates almost only from the location of the marker layer.

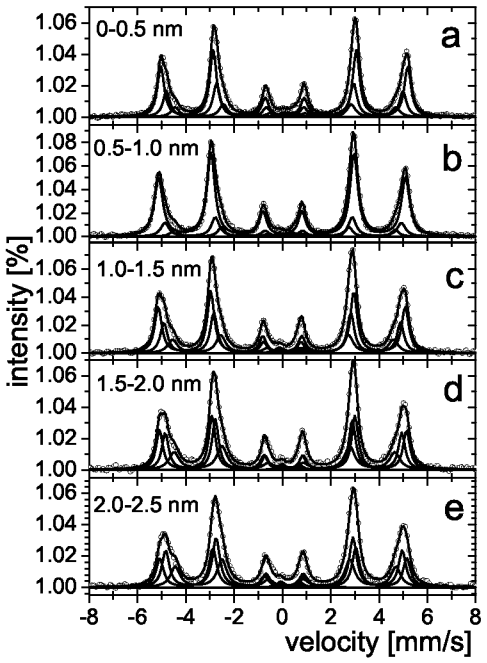

Fig. 2. CEM spectra of Ag/Fe multilayers with $\lambda = 5$ nm and a ^{57}Fe marker layer at various locations within the natural Fe layer. The position is indicated in the graph.

These spectra are again fitted with the three sextets and the doublet as before. The abundance of the doublet D is not changing within its error limits (1–2.5%). The hyperfine fields of the sextets were first fitted freely and then adjusted to their mean values, in order to achieve a better accuracy in the relative abundances of the subspectra, which are sensitively depending on the hyperfine fields. The values are 31.7 T (M0), 30.4 T (M1) and 28.4 T (M2). There are no changes in the intensity ratios within the error limits. The relative areas of the sextets are summarized in Fig. 3.

The abundances are asymmetrically changing between the Ag interfaces. The Ag content is changing reciprocally to the fraction of the M0 sextet. The maximum of the M0 fraction is obtained for the marker layer located from 0.5 to 1.0 nm. The minimum for the M0 fraction is obtained at the top Ag interface. If we assume a random distribution of the Ag atoms, we can use the binomial distribution

$$P(n,c) = \binom{14}{n} c^n (1-c)^{14-n} \tag{1}$$

to calculate the Ag concentration in the bcc-phase, which is displayed in Fig. 4.

The Ag concentration ranges from 2 at.% to 8 at.%. The behaviour of course resembles the fractions in Fig. 3, the minimum at 0.5–1.0 nm, 4 at.% at the lower interface and increasing towards 8 at.% at the upper interface.

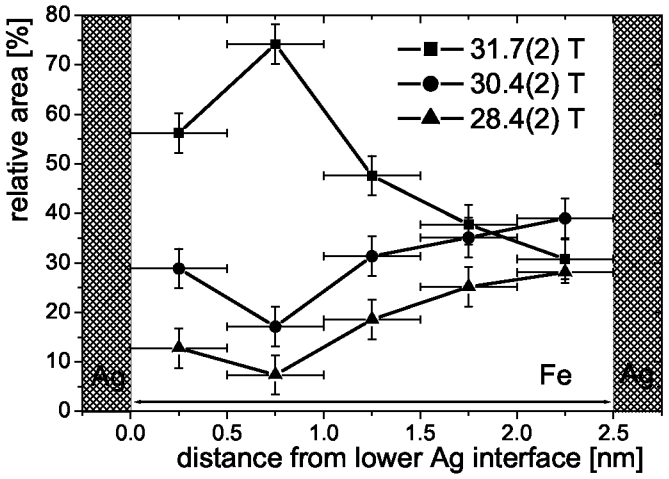

Fig. 3. Relative areas as obtained from the fits of the CEM spectra shown in Fig. 2.

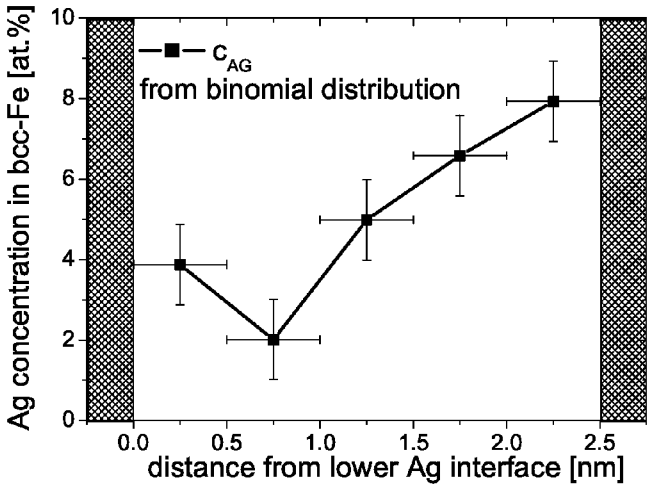

Fig. 4. Ag concentration in Fe calculated from the fractions of the sextets.

Now, the question is, how this behaviour can be explained. The energy of the deposited ions and atoms was measured to be in the range of 10–200 eV [15]. According to the theory of energy loss (nuclear and electronic stopping power) in matter [26, 27], the range of Ag deposited onto Fe and vice versa can be estimated to be 1 nm for Ag on Fe and 2 nm for Fe on Ag (at 200 eV), i.e. Fe is penetrating deeper into Ag than the Ag into Fe. Furthermore, the Ag–Fe system is highly immiscible and thus severely tending to a de-mixing of any intermixing. The mobility of Fe in Ag is higher than vice versa, therefore, the Fe is diffusing faster out of

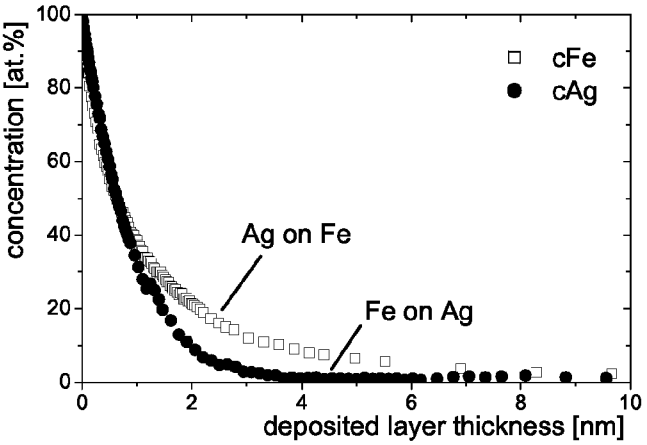

Fig. 5. AES concentration profiles for Fe deposited on top of Ag and for Ag deposited on top of Fe.

Ag than the other way around. This is verified in the AES measurement shown in Fig. 5.

It comes out that the Ag concentration is decreasing faster when Fe is deposited onto Ag than the Fe concentration when Ag is deposited onto Fe. Although the Fe is implanted deeper, the Ag is rapidly covered by a closed Fe layer, due to the higher mobility of Fe atoms out of the Ag layer, whereas the Ag remains inside the Fe layer and needs more particles to cover the Fe layer completely.

This now also explains the CEM spectra of the marker layers. At the lower Ag interface the Fe is implanted into the Ag and then diffusing outward again leaving some Ag in the lowest Fe layer. In the centre there is almost pure iron, whereas at the upper Ag-interface, the Ag is implanted into the Fe and remains there, due to the lower mobility.

These experiments are now repeated with a higher periodicity of 10 nm, in order to prove this hypothesis.

4. Conclusions

It is shown that the intermixing in multilayers can be asymmetric for the lower and upper interface due to the different implantation ranges and a different mobility of the element in its counterpart. Surprisingly, also the small implantation ranges in the order of 1 nm play an important role for the microstructure and short-range order of the interfaces.

It is also demonstrated that hyperfine interactions and a clever design of the experiments using the isotopic sensitivity and the trick of marker layers together with the preparation accuracy of the PLD process can give deep insights into material surface processes.

Acknowledgments

This work is supported by Sonderforschungsbereich SFB 345 "Festkörper weit weg vom Gleichgewicht" Göttingen.

References

[1] W.M. Steen, *Laser Material Processing*, Springer Verlag, Berlin 1998.

[2] M. von Allmen, A. Blatter, *Laser-Beam Interactions with Materials*, Springer Verlag, Berlin 1986.

[3] D. Bäuerle, *Laser Processing and Chemistry*, Springer Verlag, Berlin 2000.

[4] P. Schaaf, *Prog. Mater. Sci.* **47,** (2002), in print.

[5] P. Schaaf, C. Illgner, F. Landry, K.-P. Lieb, *Surf. Coat. Technol.* **100/101,** 404 (1998).

[6] C. Illgner, P. Schaaf, K.-P. Lieb, R. Queitsch, J. Barnikel, *J. Appl. Phys.* **83,** 2907 (1998).

[7] F. Landry, K.-P. Lieb, P. Schaaf, *J. Appl. Phys.* **86,** 168 (1999).

[8] S.B. Ogale, P.P. Patil, D.M. Phase, Y.V. Bhandarkar, S.K. Kulkarni, S. Kulkarni, S.V. Ghaisas, S.M. Kanetkar, V.G. Bhide, S. Guha, *Phys. Rev. B* **36,** 8237 (1987).

[9] E. D'Anna, G. Leggieri, A. Luches, M. Martino, A.V. Drigo, I.N. Mihailescu, S. Ganatsios, *J. Appl. Phys.* **69,** 1687 (1991).

[10] C. Illgner, K.-P. Lieb, P. Schaaf, K. Mann, H. Köster, G. Marowsky, *Appl. Phys. A* **62,** 231 (1996).

[11] C. Illgner, P. Schaaf, K.-P. Lieb, E. Schubert, R. Queitsch, H.W. Bergmann, *Appl. Phys. A* **61,** 1 (1995).

[12] F. Landry, M. Neubauer, K.-P. Lieb, P. Schaaf, in: *ECLAT98 (European Conf. Laser Treatment of Materials)*, Ed. B.L. Mordike, Werkstoff-Informationsges., Frankfurt 1998, p. 81.

[13] P. Schaaf, *Hyperfine Interact.* **111,** 113 (1998).

[14] *COLA Proceedings: Appl. Phys. A* **69,** (Suppl.) (1999); *Appl. Surf. Sci.* **127-129,** (1998); *Appl. Surf. Sci.* **96-98,** (1996).

[15] S. Fähler, H.-U. Krebs, *Appl. Surf. Sci.* **96-98,** 61 (1996).

[16] H.-U. Krebs, Y. Luo, M. Störmer, A. Crespo-Sosa, P. Schaaf, W. Bolse, *Appl. Phys. A* **61,** 591 (1995).

[17] H.-U. Krebs, *Int. J. Non-Equilibrium Proc.* **10,** 3 (1997).

[18] P. Schaaf, A. Krämer, F. Aubertin, U. Gonser, *Z. Metallkunde* **82,** 815 (1991).

[19] P. Schaaf, A. Krämer, L. Blaes, G. Wagner, F. Aubertin, U. Gonser, *Nucl. Instrum. Methods B* **53,** 184 (1991).

[20] F. Landry, P. Schaaf, WinISO fit program for Mössbauer spectra, unpublished.

[21] A. Crespo-Sosa, P. Schaaf, W. Bolse, K.-P. Lieb, M. Gimbel, U. Geyer, C. Tosello, *Phys. Rev. B* **53,** 14795 (1996).

[22] M. Neubauer, K.-P. Lieb, P. Schaaf, M. Uhrmacher, *Phys. Rev. B* **53,** 10237 (1996).

[23] M. Neubauer, K.-P. Lieb, P. Schaaf, M. Uhrmacher, *Thin Solid Films* **275,** 69 (1996).

[24] P. Schaaf, A. Crespo-Sosa, K.-P. Lieb, W. Bolse, C. Tosello, in: *Proc. Int. Conf. Applications Mössbauer Effect (ICAME), Rimini (Italy) 1995, Conf. Proc. SIF*, Ed. I. Ortalli, Vol. 50, Compositori, Bologna 1996, p. 695.

[25] P. Schaaf, C. Illgner, M. Niederdrenk, K.-P. Lieb, *Hyperfine Interact.* **95,** 199 (1995).

[26] G. Betz, K. Wien. *Int. J. Mass Spect.* **140,** 1 (1994).

[27] J.F. Ziegler, *The Stopping and Ranges of Ions in Matter*, Pergamon Press, New York 1980.